Rapidly and Automatically Estimating Reachability of Electric Propulsion Spacecraft

Prashant R. Patel[*], and Daniel J. Scheeres[†]

August 25, 2022

ABSTRACT

Reachable and controllable sets for electric propulsion spacecraft are important to many problems including: dynamic replanning, robust mission design, space situational awareness, assessing advanced concepts, and threat assessments. Current methods result in a two-point boundary value problem or are limited in their application. We solve the reachable and controllable problem by formulating it as a multi-stage indirect approach. We demonstrate that this enables rapid, reliable, and autonomous estimates of the reachable and controllable set. We show that our approach works in strong multi-body environments (i.e., flybys) and incorporate uncertainty in initial conditions. These make the algorithm suitable for space situational awareness and deep space applications.

1. INTRODUCTION

Range as a function of fuel is an important concept. It is needed for dynamic fleet replanning, context-based mission orders, robust mission design, situational awareness, autonomous operations, and designing advanced concepts such as basing versus refueling trades. In addition, uncertainty is a key factor in space as it is a driver in conjunction analysis. We incorporate initial ellipsoid uncertainty estimates into our range algorithms. This enables us to estimate the potential maneuver envelop of spacecraft while taking into account that spacecraft locations are uncertain.

Air, land, and sea have long used fuel-range calculations. Electric propulsion (EP) space systems do not have an equivalent analog. Work by Holzinger[6] derived the general equations for a continuous indirect formulation and showed that these problems can be solved. The indirect approach results in a two-point boundary value problem which is difficult to solve. Bryson and Ho characterized two-point boundary value problems as::[4]

> The main difficulty with these methods is getting started; i.e., finding a first estimate of the unspecified conditions at one end that produces a solution reasonably close to the specified conditions at the other end. The reason for this peculiar difficulty is that external solutions are often very sensitive to small changes in the unspecified boundary conditions. This extraordinary sensitivity is a direct result of the nature of the Euler-Lagrange equations,...

Bando et. al[3] use a power series expansion of the generating function to identify low thrust transfers in the Hill frame. Generating functions provide the solution flow; however, current techniques only work on dynamical systems with polynomial forms (e.g., Hill problems).[5] Thorne[10] derived a set of formulas that produce approximate values for both the initial Lagrange co-states and the associated optimal flight time needed to solve the minimum-time, continuous-thrust orbital trajectory design problem. Thorne's formulas are especially accurate for either high-thrust or short-duration transfers starting from circular conditions, but they have also been used effectively to solve low-thrust, noncircular, three-dimensional problems with the continuation method.

Our contribution is to develop a fast, scalable, and automated algorithm that can rapidly and reliably estimate the reachable and controllable set for EP spacecraft. Our algorithm does not require the need for any initial guess by users because we structure the problem to avoid the need to solve a two-point boundary value problem. In addition, we incorporate ellipsoid uncertainty[6] thereby allowing the algorithm to be used when state estimates have been derived from observational data. We test the algorithm in multi-body environments including near-lunar flybys. This demonstrates that our approach works in highly challenging dynamic environments.

We achieve these results by:

[*]Research Staff Member, Cost Analysis and Research Division, Institute for Defense Analyses, 730 Glebe Road, Alexandria VA. 22305

[†]A. Richard Seebass Chair Professor, Ann and H.J. Smead Aerospace Engineering Sciences, University of Colorado, 3775 Discovery Drive, Boulder CO 80303

- Formulating the reachable problem as an indirect multi-stage problem
- Writing the cost function in a linear form
- Structuring the optimal control problem so that a non-thrusting trajectory is a valid solution

We begin by reviewing the multi-stage formulation and discuss notation. Next, we derive the specific equations used in our formulation of the reachable problem. We then show how this formulation can be rapidly and automatically solved with several examples on consumer hardware.

2. INDIRECT MULTI-STAGE FORMULATION AND NOTATION

We consider a controlled dynamical system defined by:

$$\dot{x} = f(x,t,u,p) \tag{1}$$

Where a *bold* indicates a vector or matrix while a *normal* font indicates a scalar quantity. x represents the state vector; u is the control vector, which is in general a function of time; t is time, and p are a set of parameters that are constant in the system.

This system can be transformed into a set of indirect multi-stage formulation equations.[4] A trajectory segment i is governed by:

$$x^{i+1} = F^i(x^i,t^i,u^i,p) \tag{2}$$

where

$$F^i = x^i + \int_{t_i}^{t_{i+1}} \dot{x}dt = x^i + \int_{t_i}^{t_{i+1}} f(x,t,u,p)dt \tag{3}$$

A trajectory is then composed of a series of N trajectory segments, where $N \geq 1$. For a multi-segment trajectory we can integrate Eq. (2) from i to $i+1$, then recursively use $i+1$ to obtain $i+2$ and so on. In our current formulation, within each segment the controls $u(i)$ are fixed. This is not a significant limitation as time varying inputs can be modeled by having $u(i)$ specified by constant coefficients to a time varying function.

The cost function for a multi-stage formulation is given by:

$$J = \phi(x^N,N) + \sum L(i,x^i,u^i) \tag{4}$$

where $\phi(x_N,N)$ is the terminal cost function and $L(i,x,u) = L^i$ are the integral cost function evaluated at the ith step. This leads to a Hamiltonian of:

$$H = \sum H^i \tag{5}$$

$$H^i = \lambda^{i+1} \cdot F^i + L^i + \sum_k \nu_k C_k \tag{6}$$

For notational convenience later, we specify the adjoints with an index $i+1$, and C represents the per stage constraints.

Taking the partial with respect to x yields the dynamics equations for the co-states.

$$H_x^i = \lambda^i = F_x^{iT}\lambda^{i+1} + L_x^i + \sum_k \nu_k C_{k,x} \tag{7}$$

where T is the transpose operator. The control law is then given by Pontryagin's principle, here by taking the partial of the Hamiltonian with respect to the control and solving for when this is zero and hence an extremal. This is:

$$H_u^i = 0 = F_u^{iT}\lambda^{i+1} + L_u^i + \sum_k \nu^k C_u^k \tag{8}$$

The initial and terminal conditions are given as:

$$C^0(x) = 0 \quad C^N(x) = 0 \tag{9}$$

which result in the initial and terminal co-states being:

$$\lambda^0 = \nu^0 \cdot C_x^0 \quad \lambda^N = \phi_x + \nu^N \cdot C_x^N \tag{10}$$

Taken together, these represent the general equations for the multi-stage optimization problem. Next, we specify our particular formulation.

3. REACHABLE EQUATIONS

The equations of motion we use in this paper are stated in an inertial frame with an arbitrary origin:

$$\dot{x} = \begin{bmatrix} \dot{r} \\ \dot{v} \\ \dot{n} \end{bmatrix} = \begin{bmatrix} v \\ \sum_j -\frac{\mu^j}{|r-r^j|^3}(r-r^j) + nT \\ n^2 \frac{T_{mag}}{c} \end{bmatrix} \tag{11}$$

where μ_j is the gravitational parameter of the attracting body located at r_j, T is the thrust vector, T_{mag} is the magnitude of thrust, r is the position vector, v is the velocity, n is the inverse mass, and c is one Earth gravity times the specific impulse. The cost function is defined as:

$$J = -min \quad \hat{z} \cdot x^N \tag{12}$$

This represents maximizing x^N along the direction $\hat{z}$, which is a specified vector which will be swept over to sample the reachable set. We also require that $|T| = T_{mag}$ and $0 \leq |T| \leq T_{max}$. These conditions require the thrust must be less than the maximum allowable thrust, T_{max}, and that the total thrust and T_{mag} are equal. The latter simply enforces the constraint that the thrust used to generate acceleration is equal to the thrust supplied by the engine.

The Hamiltonian is then:

$$H^i = F^{iT} \lambda^{i+1} + \nu_1(|T| - T_{mag}) + \nu_2(\frac{1}{2}T_{mag}^2 - \frac{1}{2}T_{max}^2) \tag{13}$$

The co-state equation is:

$$H_x^i = \lambda^i = {F_x}^{iT} \lambda^{i+1} \tag{14}$$

and is formulated to move backwards in time. The term F_x^i is the state transition matrix at the end of the segment. It is given by

$$F_x^i = \frac{\partial x^{i+1}}{\partial x^i} = \Phi(t^{i+1}, t^i) = \int_{t^i}^{t^{i+1}} \begin{bmatrix} 0 & I & 0 \\ \frac{\partial \dot{v}}{\partial r} & 0 & T \\ 0 & 0 & 2n\frac{T_{mag}}{c} \end{bmatrix} \Phi(t, t^i) dt \tag{15}$$

where Φ is the state transition matrix. The initial conditions for $\Phi(i,i) = I$

The control law is defined by:

$$H_u = 0 = {F_u}^{iT} \lambda^{i+1} + \nu_1 \begin{bmatrix} \frac{T}{|T|} \\ -1 \end{bmatrix} + \nu_2 \begin{bmatrix} 0 \\ T_{mag} \end{bmatrix} \tag{16}$$

and

$$F_u^i = \frac{\partial x^{i+1}}{\partial u^i} = \Omega(t^{i+1}, t^i) = \int_{t^i}^{t^{i+1}} \begin{bmatrix} 0 & I & 0 \\ \frac{\partial \dot{v}}{\partial r} & 0 & T \\ 0 & 0 & 2n\frac{T_{mag}}{c} \end{bmatrix} \Omega(t, t^i) + \begin{bmatrix} 0 & 0 & 0 & 0 \\ - & diag(n) & - & 0 \\ 0 & 0 & 0 & \frac{n^2}{c} \end{bmatrix} dt \tag{17}$$

The term Ω is analogous to the impulse response matrix for linear systems. The initial condition for the integral is given by $\Omega(i,i) = 0$. Solving Eq. (16) and satisfying the constraints results in:

$$T_{mag} = T_{max}, \quad and \quad T = -T_{max} \frac{{F_T}^T \lambda}{|{F_T}^T \lambda|} \tag{18}$$

where

$$\nu_1 = \left| {F_T}^T \lambda^{i+1} \right| \tag{19}$$

$$\nu_2 = \frac{\nu_1 - F_{T_{mag}}^T \lambda^{i+1}}{T_{max}} \tag{20}$$

In these equations F_T is the columns of F_u associated with the thrust direction T. Similarly, $F_{T_{mag}}$ is the column of F_u associated with T_{mag}.

We can also account for initial state uncertainty. We can use the same formulation that is used by Holzinger.[6]

$$C^0 = \frac{1}{2}\delta x_0^T E \delta x_0 - \frac{1}{2}d^2 \tag{21}$$

$$C_x^0 = E\delta x_0 \tag{22}$$

Where E is a symmetric full rank matrix and with d defines the ellipsoid set that the initial states lie on. Combining these equations we get

$$\delta x_0 = -d\frac{E^{-1}\lambda_0}{\sqrt{\lambda_0^T E^{-1}\lambda_0}} \tag{23}$$

In cases where there is uncertainty in only some of the states or the uncertainty is decoupled (e.g., position or velocity) then Eq. (23) is still valid but would be applied to those sub-elements only. For example, if there is uncertainty in position estimates but not velocity then Eq. (23) would be applied to the positional states.

Additionally, we can use a similar formulation to account for initial ΔV maneuvers.

$$C^1 = \frac{1}{2}\Delta V^T \Delta V - \frac{1}{2}\Delta V_{max}^2 \tag{24}$$

$$C_x^1 = \Delta V \tag{25}$$

$$\delta v_0 = \Delta V = -\Delta V_{max}\frac{\lambda_v}{|\lambda_v|} \tag{26}$$

Because the magnitude of the ΔV maneuver is equal to ΔV_{max} we do not need a constraint for the mass. It can simply be set to the post-ΔV value.

We know have sufficient information to estimate the reachable and controllable set even when the states are uncertain. One interesting feature is that T_{max}, see Eq. (18), does not affect the direction of thrust. This allows us to integrate along the unpowered trajectory then conduct trade studies by sweeping over various thrust levels.

4. FAST FIRST ORDER ESTIMATE (FFOE) SOLUTION

We first develop a Fast First Order Estimate (FFOE) of the reachable set. This solution provides a good estimate of the reachable set. We begin by recognizing that the non-thrusting solution with $T = 0$ and $T_{mag} = 0$ can be considered an optimal solution with a zero reachability set. We can then compute the unpowered trajectory and partials (F_x and F_u) for this trajectory. We then select the values of $\hat{z}$ from a unit ball and compute the control law from Eq. (18). The final step is to integrate Eq. (11) using the derived control law to compute the reachable set under this linearization assumption. This is more formally shown in Alg. (1)

Starting with an unpowered trajectory has several practical benefits. It eliminates the need for a user supplied initial guess. The updated thrust laws can be computed using a series of matrix multiplications without requiring additional integrations. As we will show in the Example section, this method is very fast as it reduces the number of first order integrations required to 1 and requires N integrations of the equations of motion, where N is the number of points on the reachable set.

5. OPEN-LOOP EXACT (OLE) SOLUTION

The open-loop exact (OLE) solution is an open-loop method that iteratively updates the control law until the change in cost function is small. The OLE algorithm is initialized using the FFOE for a given $\hat{z}$. Then the trajectory and partials are numerically integrated and recomputed along the previous control law, using Eq. (18). The difference between the prior and current cost function is then compared. If the change in cost function between iterations is less than a specified precision the algorithm terminates. This is equivalent to terminating when the gradient along the constraint is small.

Algorithm 1 FFOE algorithm

$x^0 \leftarrow$ initial conditions
$t^0 \leftarrow$ start time
$dt \leftarrow$ segment duration
$Seg \leftarrow$ number of segments
$T \leftarrow 0$
$i \leftarrow 0$
while $i < Seg$ **do**
    $x^{i+1}, {F_x}^i, {F_u}^i \leftarrow F^i(x^i, T^i, t_0, t_0 + dt)$
    $t_0 \leftarrow t_0 + dt$
    $i \leftarrow i + 1$
end while
$j \leftarrow 0$
$N \leftarrow$ Number of sample points
while $j < N$ **do**
    $i \leftarrow Seg - 1$
    $\lambda^{Seg} \leftarrow$ from unit ball
    while $i \geq 0$ **do**
        $T^{i,j} \leftarrow$ Eq. (18)
        $\lambda^i \leftarrow$ Eq. (14)
        $i \leftarrow i - 1$
    end while
    $j \leftarrow j + 1$
end while
$j \leftarrow 0$
while $j < N$ **do**
    $i \leftarrow 0$
    while $i < Seg$ **do**
        $x^{i+1} \leftarrow F^i(x^i, T^{i,j}, t_0, t_0 + dt)$
        $t_0 \leftarrow t_0 + dt$
        $i \leftarrow i + 1$
    end while
    $j \leftarrow j + 1$
end while

6. EXAMPLES

In this section we provide various examples to highlight the performance and utility of the algorithms. For these examples we code the equations in C++ on an M1 MacBook Pro from 2020. We use the Boost Libraries for integration. In particular, we use a Fehlberg 78 order integrator with error tolerances $\leq 10^{-13}$. We use Armadillo[8,9] for matrix/vector support. We also use the JPL SPICE libraries[1,2] and DE440 ephemerides.[7] Plotting is done in spacekit.js[1]. Parallel processing is done by leveraging the BOOST ASIO library. The reference frame is ECLIPJ2000, the specific impulse is set to 3000 seconds, and the Sun, Earth, and Moon are gravitating.

We show three examples to demonstrate the uses of the algorithm. Case 1 is a reachability case with an elliptic orbit around Earth with no significant multi-body effects. The goal of case 1 is to show how the FFOE and OLE compare to one another. Case 2 is also a reachability case with a lunar flyby. This shows that the FFOE algorithm works well with strong multi-body interactions. For case 3, we run case 2 as a controllability problem. This highlights the initial envelope that a spacecraft can start in and still reach the terminal states.

6.1 Case 1

The first case represents a relatively straightforward reachability case. The initial orbit is an elliptical trajectory with no significant multi-body effects. The simulation parameters are a max thrust of 0.01 N, 200 segments, and segment duration of 7200 seconds.

We compute the reachable set using the first order methods and the open-loop method. We see both the FFOE solution and OLE solution produce similar results, see Fig. (1). The computational time is 0.27 seconds and 4.32 seconds respectively.

6.2 Case 2

The second case is a multi-body reachability case. The trajectory has a close approach to the moon. This results in strong multi-body effects and an inclination and energy increase. The first order method does a fairly good job; however, we see that the exact method captures the edges better, see Fig. (2). In Fig. (3) we can see the entire trajectory projected onto the X-Y plane relative to the Earth and Moon.

The simulation parameters are a max thrust of 0.02 N, 200 segments, and segment duration of 7200 seconds. The computation time of the FFOE and OLE algorithms is 0.25 seconds and 6.42 seconds respectively. Fig. (4) and Fig. (5) highlight the three dimensional nature of the trajectories by showing the close approach and inclination change.

6.3 Case 3

For the third case, we start at the end of case 2 and run it backwards. This is a controllability case and shows the range of initial conditions that would allow the spacecraft to still reach the terminal state. The simulation parameters are a max thrust of 0.02 N, 200 segments, and segment duration of -7200 seconds. Fig. (6) shows the simulation results. We see that the trajectory is the same as case 2. For the controllability problem, we identified the envelope of initial conditions that enable the final states in case 2 to be reached.

6.4 Case 4

The fourth case is is the same as case two with uncertain initial conditions. We assume only the position is uncertain and that it lies on a 500 km unit sphere. The initial uncertainty envelope is visualized in Fig. (7) while the reachable set is shown in Fig. (8).

6.5 Case 5

The fifth case is is the same as case three (controllability example) with uncertain initial conditions. We assume only the position is uncertain and that it lies on a 5000 km unit sphere. The initial uncertainty envelope is visualized in Fig. (9). The XY view of the reachable set is shown in Fig. (10) and Fig. (11) shows how with uncertainty the controllable set is contorted and expanded.

7. ADDITIONAL APPLICATIONS

The authors are extended the this work to be able to handle fuel-minimum trajectories. This will allow the algorithm to estimate the reachable/controllable set but also interior feasible solutions.

[1] https://typpo.github.io/spacekit/

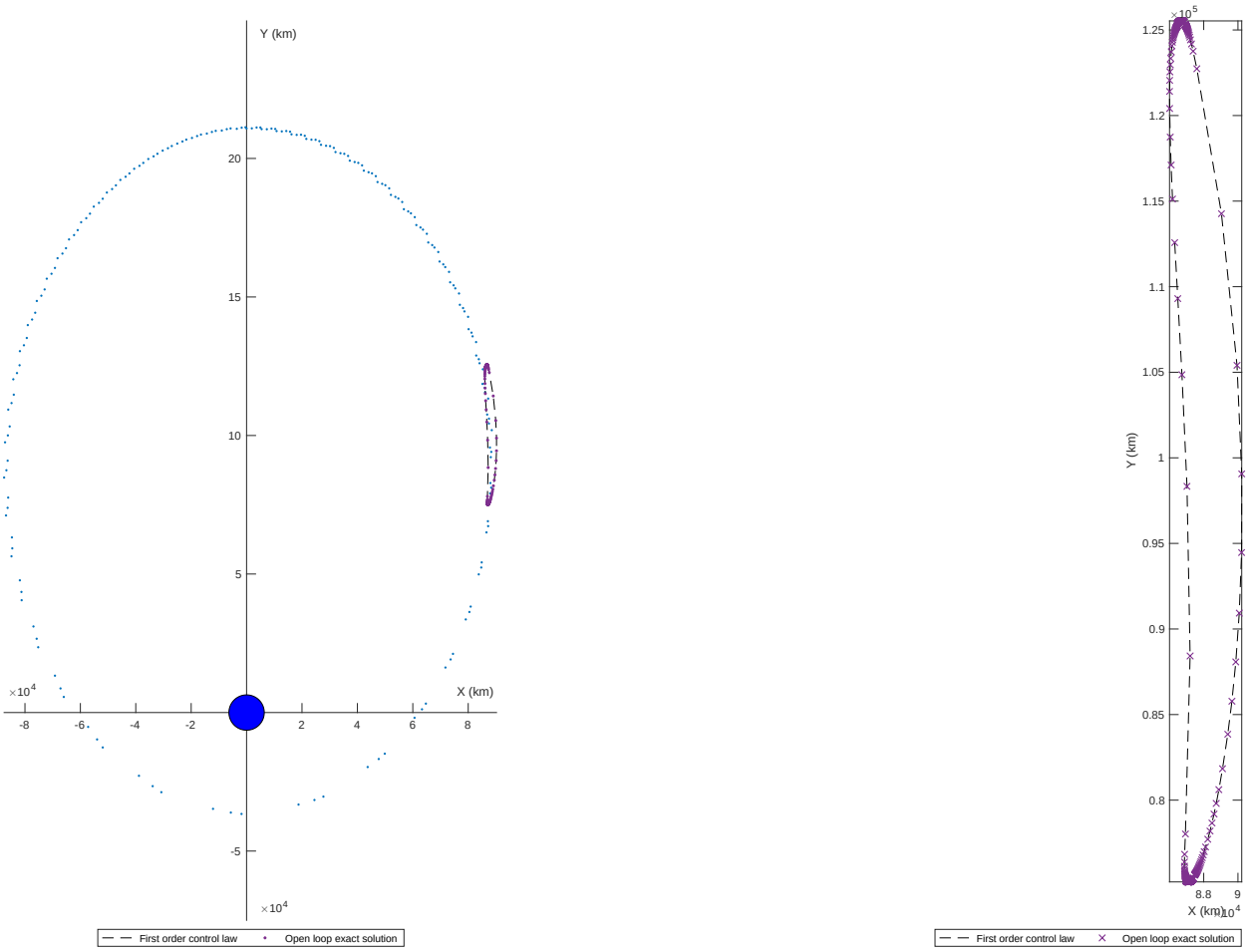

Fig. 1: Elliptic trajectory around Earth. No significant multi-body interaction. The epoch and initial conditions are 64.1 seconds and $x^0 = [0, 210820, 0, 0.753136347, 0, 0, 1000]$ Units are km, km/s, and kg.

8. CONCLUSION

We demonstrate a fast and automated algorithm to estimate the reachable and controllable set for EP spacecraft. We show that the algorithm works in multi-body cases and can account for uncertainty in initial conditions. This makes it useful for space domain awareness applications to include deep space. Our algorithm is fast and scales through the use of parallel/concurrent processing.

9. ACKNOWLEDGEMENTS

The authors would like to thank Jim Thorne, Greg Davis, and Stefania Brown-VanHoozer for providing valuable suggestions that helped improve this work. We would also like to thank Dr. Lindsay Millard for bringing this problem to our attention. The Institute for Defense Analyses (IDA) graciously provided funding to publish and present this work.

REFERENCES

[1] Charles Acton, Nathaniel Bachman, Boris Semenov, and Edward Wright. A look towards the future in the handling of space science mission geometry. *Planetary and Space Science*, 150:9–12, 2018.

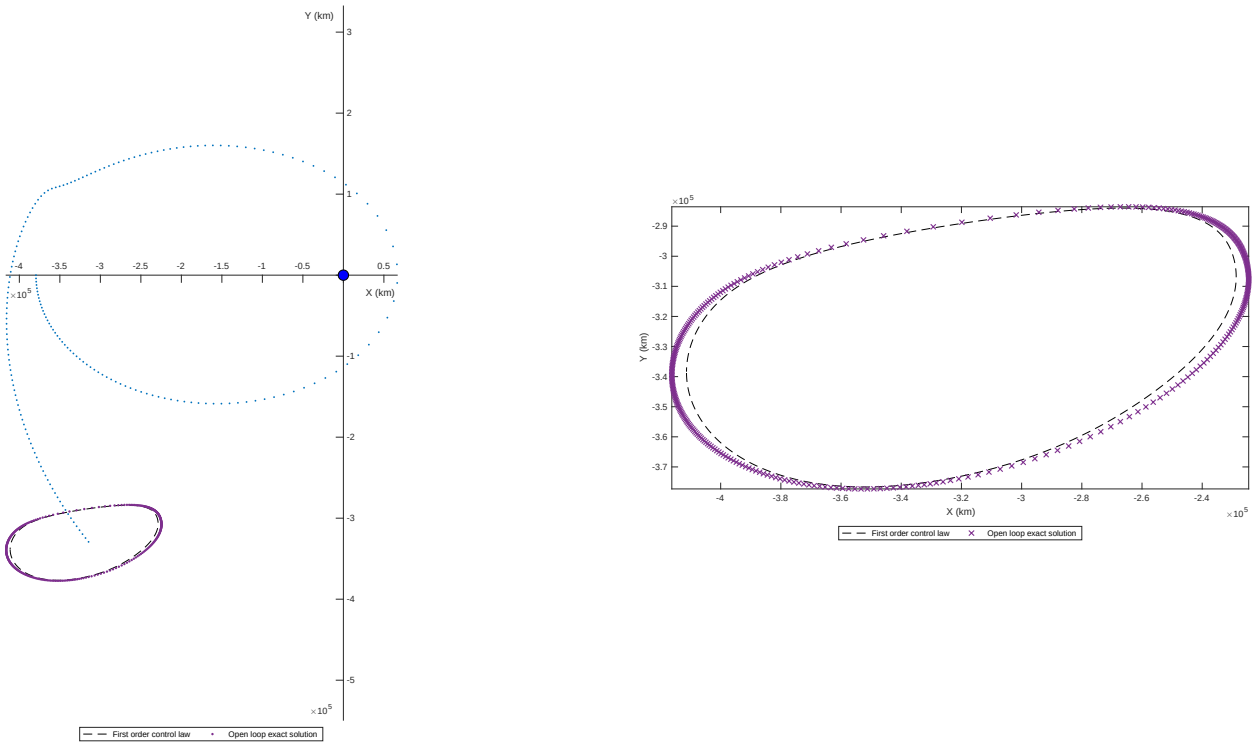

Fig. 2: Earth-Sun-Moon gravitating. We show good agreement between the FFOE and OLE algorithm. The OLE solution shows that the extreme edges are underestimated by the FFOE algorithm. The epoch and initial conditions are 1072864.169 seconds and $x^0 = [-379476, 0, 0, 0, -0.561354689, 0, 1000]$. Units are km, km/s, and kg.

[2] Charles H Acton Jr. Ancillary data services of nasa's navigation and ancillary information facility. *Planetary and Space Science*, 44(1):65–70, 1996.

[3] Mai Bando and Daniel J Scheeres. Nonlinear attractive and reachable sets under optimal control in three-body problem. *Journal of guidance, control, and dynamics*, 41(8):1766–1775, 2018.

[4] Arthur E Bryson and Yu-Chi Ho. *Applied optimal control: optimization, estimation, and control*. Routledge, 2018.

[5] Pini Gurfil. *Modern astrodynamics*. Elsevier, 2006.

[6] Marcus J Holzinger and Daniel J Scheeres. Reachability results for nonlinear systems with ellipsoidal initial sets. *IEEE transactions on aerospace and electronic systems*, 48(2):1583–1600, 2012.

[7] Ryan S Park, William M Folkner, James G Williams, and Dale H Boggs. The jpl planetary and lunar ephemerides de440 and de441. *The Astronomical Journal*, 161(3):105, 2021.

[8] Conrad Sanderson and Ryan Curtin. Armadillo: a template-based c++ library for linear algebra. *Journal of Open Source Software*, 1(2):26, 2016.

[9] Conrad Sanderson and Ryan Curtin. An adaptive solver for systems of linear equations. In *2020 14th International Conference on Signal Processing and Communication Systems (ICSPCS)*, pages 1–6. IEEE, 2020.

[10] James D Thorne and Christopher D Hall. Minimum-time continuous-thrust orbit transfers. *The Journal of the astronautical sciences*, 45(4):411–432, 1997.

Fig. 3: Visualization of simulation results in X-Y plane with Earth, Moon, and spacecraft reachable set.

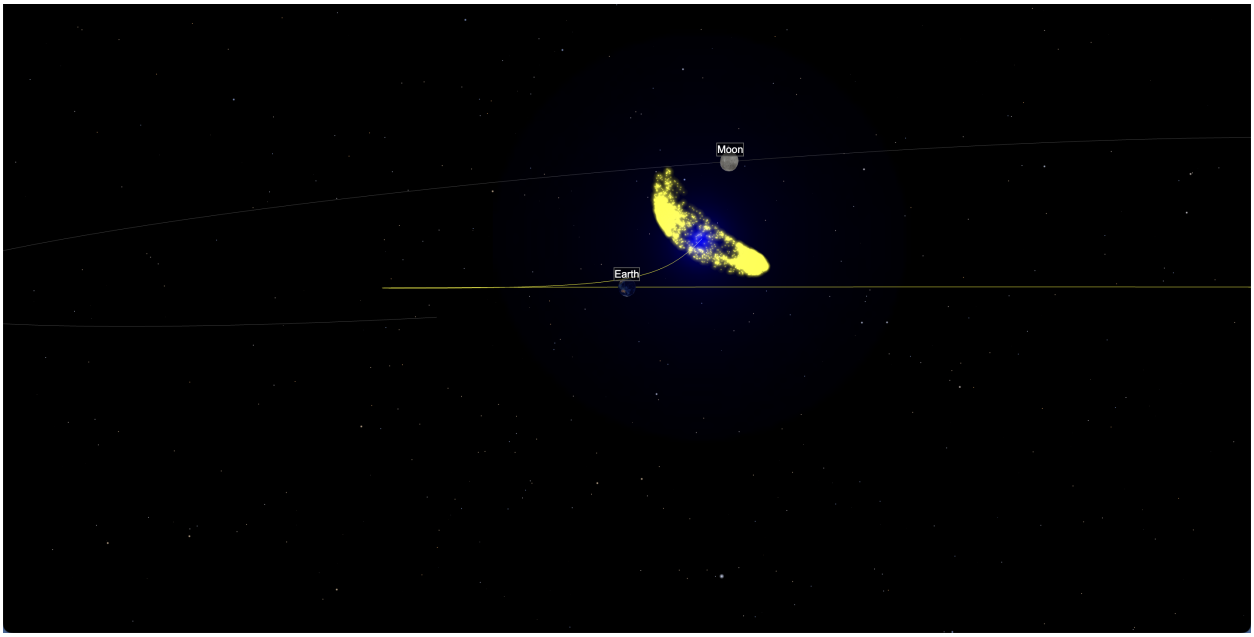

Fig. 4: Near moon interaction during flyby for case 2.

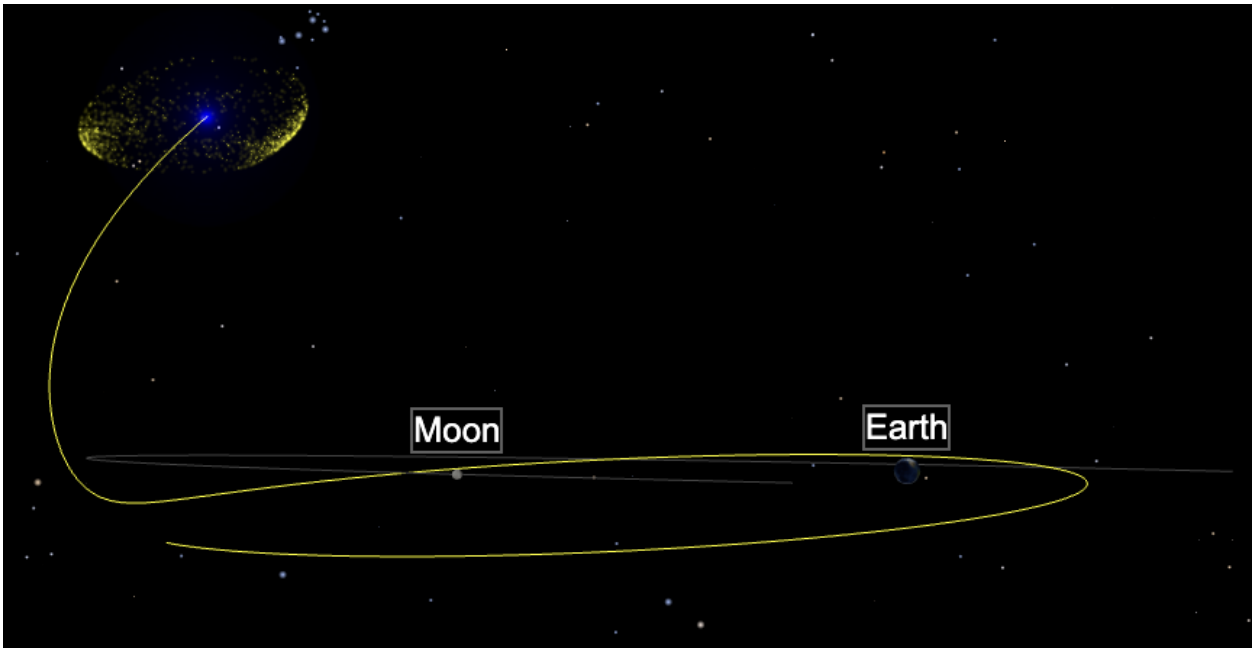

Fig. 5: 3D view to highlight inclination change of case 2 post flyby.

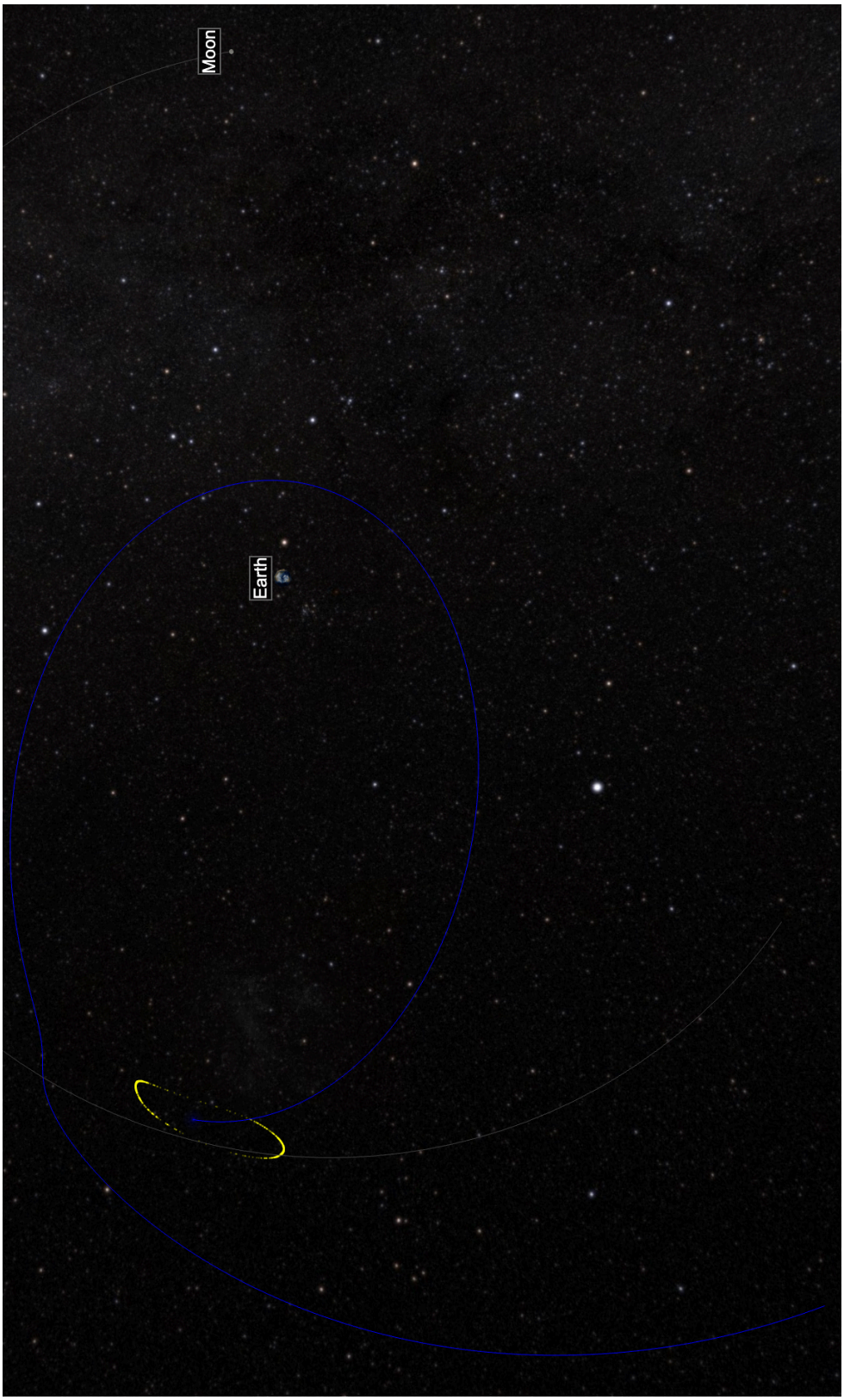

Fig. 6: Earth-Sun-Moon gravitating. Controllability case that shows the initial conditions that can result in the terminal conditions for case 2. The epoch and initial conditions are 2512864.169 seconds and $x^0 = [-314562.64, -329219.31, 237676.53, 0.5262560, -0.65552567495712999, 0.1763679, 1000.0]$. Units are km, km/s, and kg.

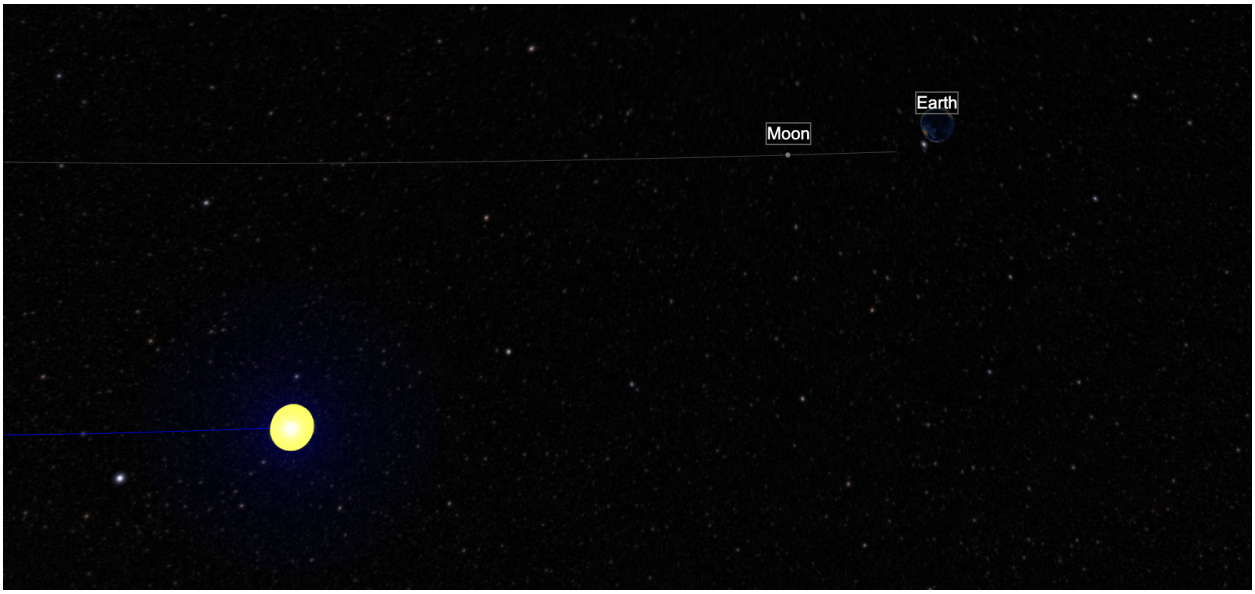

Fig. 7: Earth-Sun-Moon gravitating. This figure shows that the uncertainty range early in the trajectory.

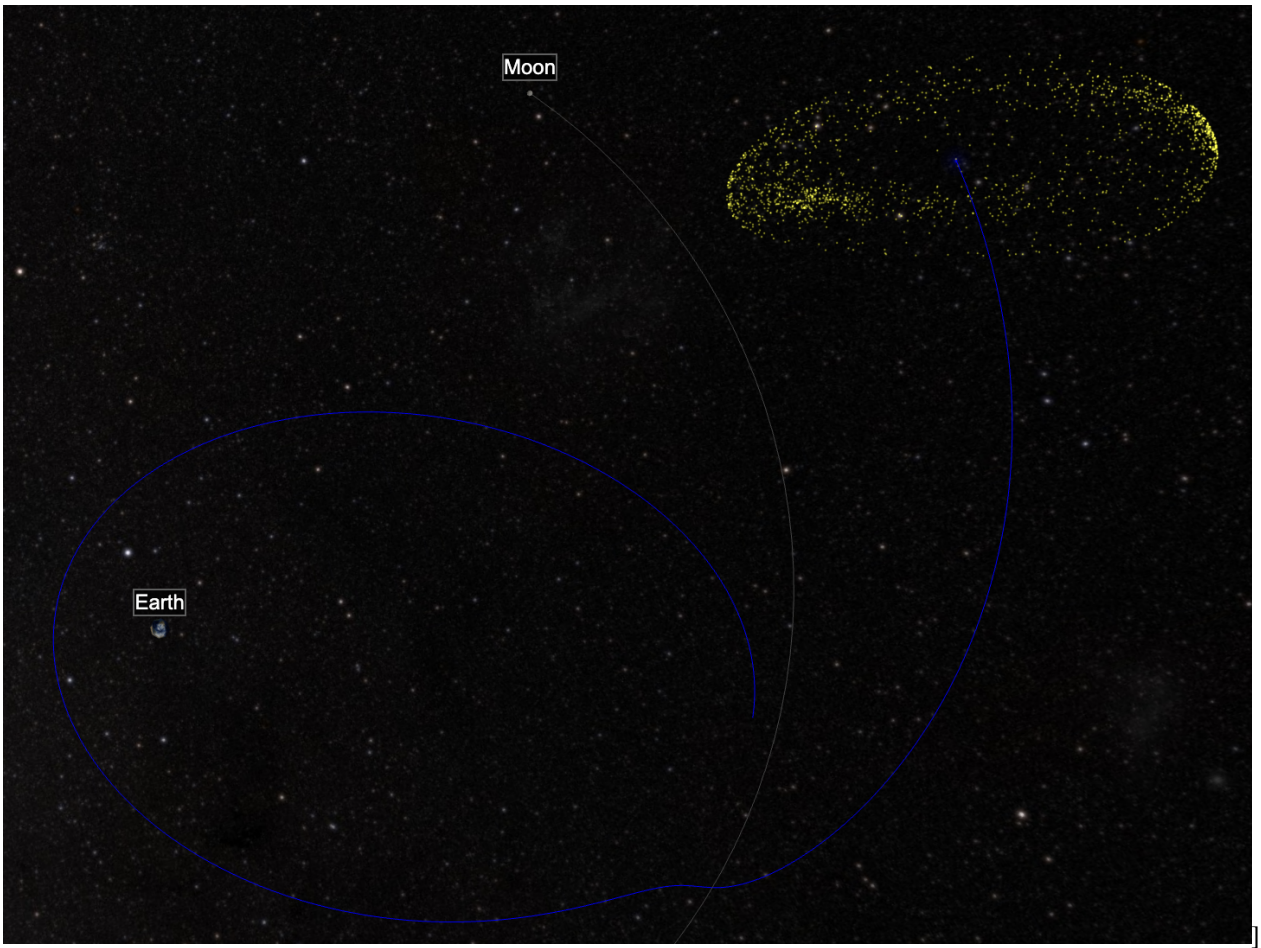

]

Fig. 8: Visualization of end of the simulation results for case 4.

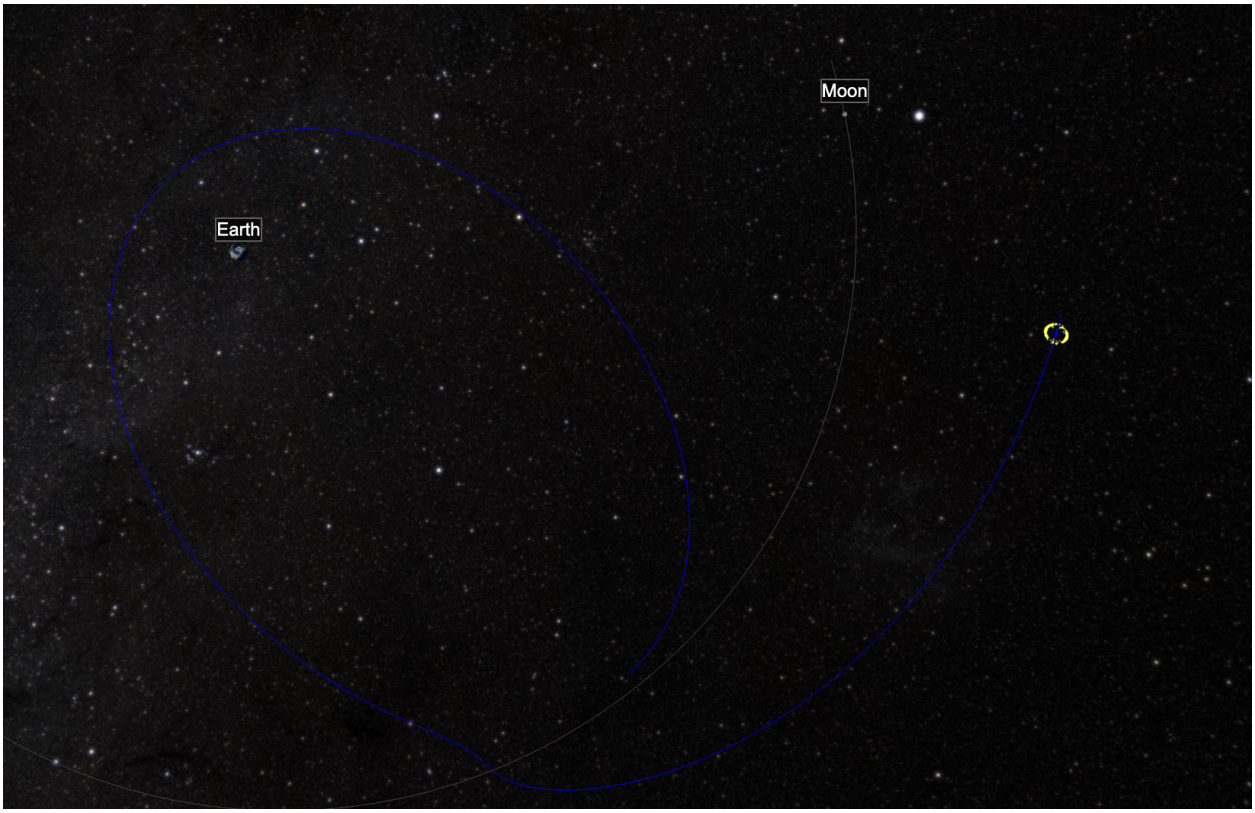

Fig. 9: Earth-Sun-Moon gravitating. This figure shows that the uncertainty range early in the trajectory.

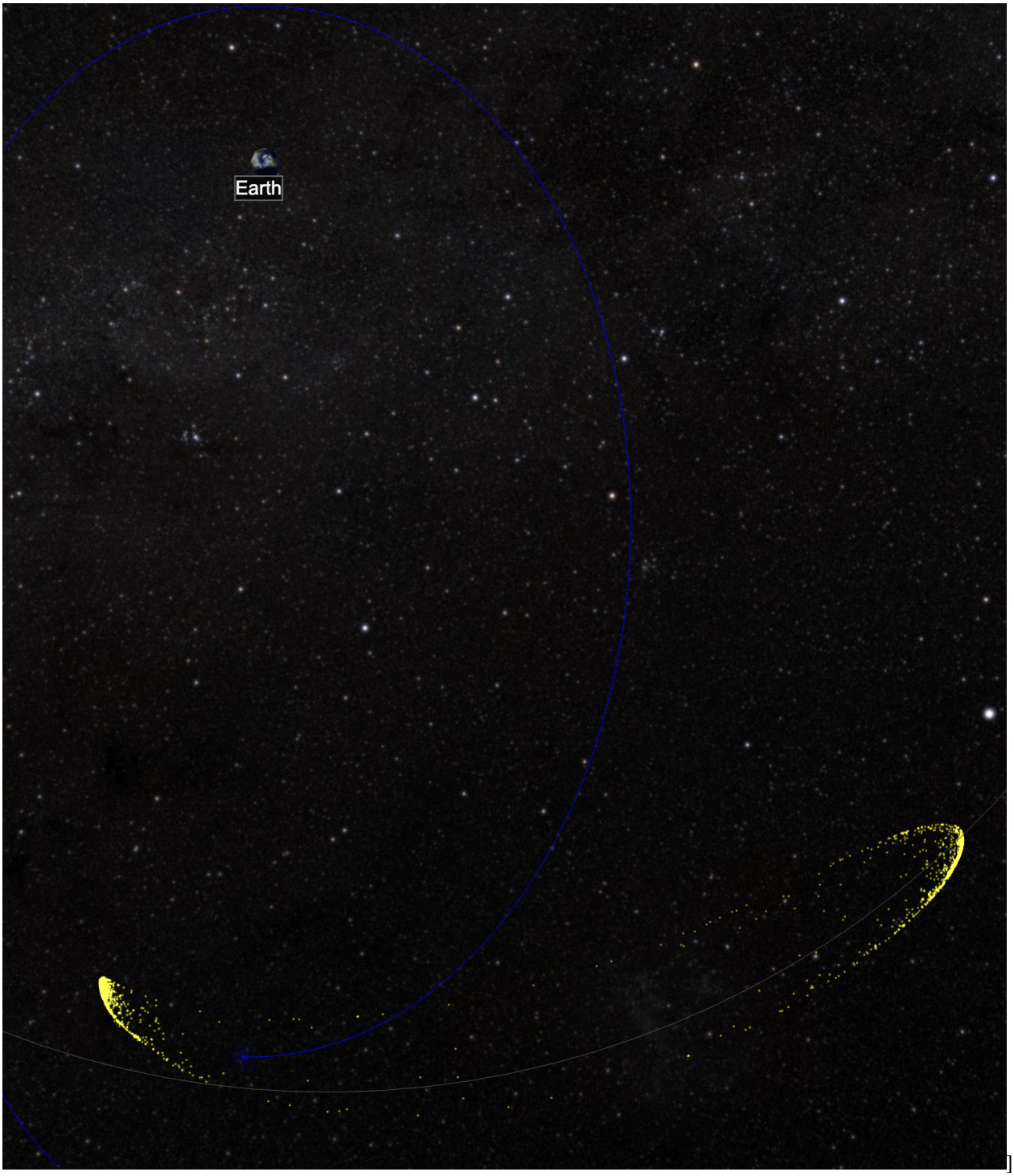

Fig. 10: Visualization of end of the simulation results for case 5 projected onto XY plane.

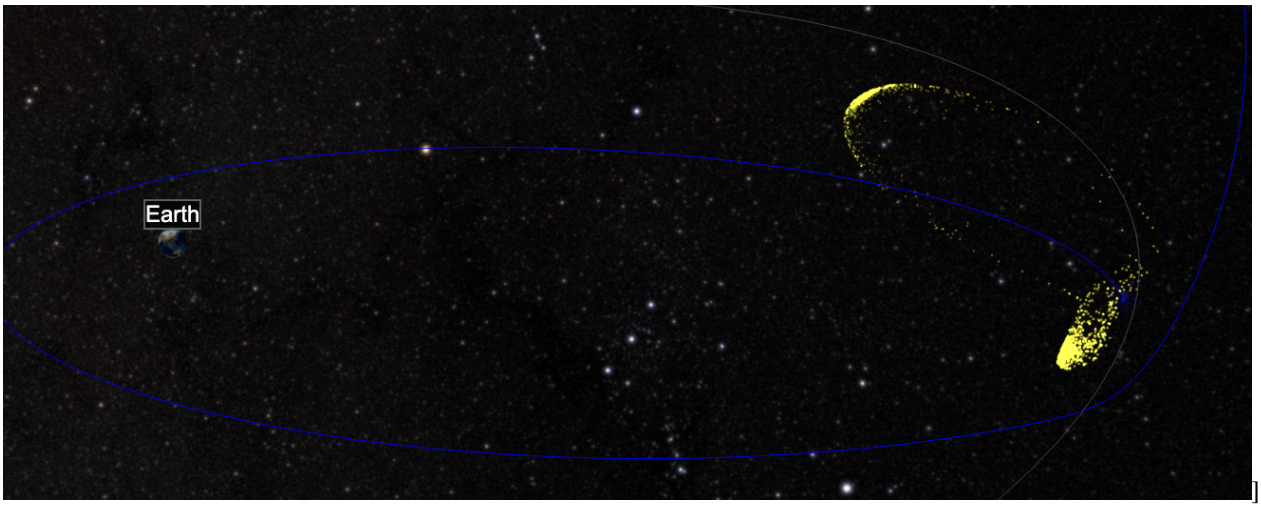

]

Fig. 11: Skewed view to highlight the contorted nature of the controllable set.